J. Fluid Mech. (1987), *vol.* 175, *pp.* 447–461
Printed in Great Britain

On the relevance of the potential-difference method for turbulence measurements

By A. TSINOBER, E. KIT AND M. TEITEL

Department of Fluid Mechanics and Heat Transfer, Faculty of Engineering, Tel-Aviv University, Ramat Aviv, Tel-Aviv, 69978, Israel

(Received 17 March 1986)

Precise theoretical relations between statistical characteristics of turbulent velocity and an electrical field are found for homogeneous and isotropic turbulence in the presence of a uniform magnetic field. These include turbulence intensities, correlations and spectra and relations allowing estimation of the degree of anisotropy of a turbulent flow. The theoretical results are verified by experiments with flow of very dilute salted water past a grid in the presence of a uniform magnetic field. The theoretical and the experimental results are in good agreement. Preliminary results of vorticity measurements are also presented.

1. Introduction

The purpose of induction velometry is to deduce a velocity $\boldsymbol{u} = [u_i]\,(i = 1, 2, 3)$ from the measurements of an electrical field $\boldsymbol{e} = [e_i] = [\partial\phi/\partial x_i]$ induced by the motion of an electrically conducting fluid in the presence of an external magnetic field $\boldsymbol{B}$, (see Shercliff 1962 and Baker 1983 for a comprehensive description of the method and a review, and recent publications by Ricou & Vives 1982, Weissenfluh 1985; Lancaster 1985, and references therein).

In the following it is assumed that the conductivity of the fluid is constant and large, the frequencies in the flow are not very large and the magnetic Reynolds number is small, i.e. that $\epsilon(\sigma T)^{-1} \ll 1$, $\sigma\mu_0 L^2 T^{-1} \ll 1$ and $\mu_0 \sigma V L \ll 1$, where V, L, T are the characteristic scales of velocity, length and time respectively, ϵ is the permittivity of the electrolyte and μ_0 the permeability of free space. These conditions are usually well fulfilled for electrolytes and liquid metals up to frequencies at least as large as $10^5\ \mathrm{s}^{-1}$. Under these conditions Ohm's law in the form

$$\boldsymbol{j} = \sigma(\boldsymbol{e} + \boldsymbol{u} \times \boldsymbol{B}) \tag{1}$$

is valid, the electrical field is a potential one, $\boldsymbol{e} = -\operatorname{grad}\phi$, and the induced magnetic field is negligible. The external magnetic field is supposed to be uniform and stationary, though many of the results presented remain valid for a non-homogeneous and/or time-dependent imposed magnetic field.

As pointed out by many authors (Grossman, Li & Einstein 1958; Shercliff 1962; Kit 1970 and others) the main difficulty of the induction-velometry method is the problem of Ohm's losses. The quantity $\boldsymbol{u} \times \boldsymbol{B}$ cannot be measured precisely unless the current $\boldsymbol{j} = 0$ or is small in comparison with either $\boldsymbol{u} \times \boldsymbol{B}$ or $-\sigma \operatorname{grad}\phi$. This occurs in some special cases, as for example in two-dimensinal flow with the magnetic field perpendicular to the plane of the flow. On the other hand, for a two-dimensional flow

with the magnetic field parallel to the plane of the flow the electrical field is constant and is defined by the flow rate (or the velocity at infinity) and the characteristics of the external electrical circuit. Therefore it is impossible to measure any local characteristics.

Thus in general the measured electric field $-\nabla\phi$ cannot be considered as $\boldsymbol{u}\times\boldsymbol{B}$. As was pointed out by Shercliff (1962, pp. 88–89) 'This is particularly important when measurements of turbulent velocities are being attempted by induction velometry .... The question as to how measurements of fluctuating electric fields and their correlations in turbulent shear flow or even in homogeneous turbulence under a uniform imposed magnetic field can be related to the statistical kinematic properties of the turbulence has not yet been answered, but certainly deserves investigation.'

In fact there is little hope of obtaining this relation in the general case of three-dimensional non-homogeneous non-isotopic turbulent flow since the electrical field is uniquely defined by only one component of vorticity (the one parallel to the magnetic field) and the boundary conditions. This follows from the equation $\operatorname{div}\boldsymbol{j}=0$ and Ohm's law (1) from which follows the Poisson equation for the electrical-field potential:

$$\nabla^2\phi = \operatorname{div}(\boldsymbol{u}\times\boldsymbol{B}) = \boldsymbol{B}\cdot\boldsymbol{\omega}, \tag{2}$$

where $\boldsymbol{\omega}=\operatorname{rot}\boldsymbol{u}$. Thus the electric field does not 'feel' the two other vorticity components of the flow field, which are perpendicular to the magnetic field. Therefore, the only information about the flow field that could be obtained from the electrical-field measurements, is that which follows from the knowledge of ω_B. It is clear that in flows where ω_B is the only component of vorticity not zero, measurements of the electrical field enable precise information on the velocity field to be obtained, as for the above-mentioned exmple of two-dimensional flow when $\boldsymbol{\omega}\parallel\boldsymbol{B}$, and $e_1=Bu_3, e_3=-Bu_1$. On the other hand, in the case of two-dimensional flow such that $\boldsymbol{\omega}\perp\boldsymbol{B}, \nabla\phi=$ const. and no local information about the flow field can be obtained.

It follows from the above arguments that, in general, calibration of a potential-difference probe consisting, for example, of two electrodes is meaningless. An exception seems to be the case when the imposed magnetic field is strongly localized in the region around the electrodes (Ricou & Vives 1982; Weissenfluh 1985).

In this work we deal with the case of homogeneous and isotropic turbulence, in which the components of velocity, vorticity, etc. are statistically the 'same'. For this reason it is possible to obtain precise relations between statistical characteristics of velocity and electrical fields. These relations are checked experimentally.

Another important application of the potential-difference method was suggested by Grossman *et al.* (1958). They pointed out on the basis of (2) that utilizing a central-difference approximation of the Laplacian of the electric potential, measured with a probe with seven electrodes, the component of vorticity parallel to the direction of the magnetic field could be obtained. The first qualitative attempt to implement this method was made by Baker (1971) using a five-electrode probe in a laminar flow. Preliminary turbulence measurements of this kind are presented here.

2. Theoretical results

2.1. *Definitions and basic relations*

In the following, the magnetic field $\boldsymbol{B}$ is supposed to be homogeneous and directed along one of the coordinate axes x_i $(i=1,2,3)$. We denote by ϕ_i the potential of the electric field normalized by B and corresponding to the magnetic field parallel to x_i.

Hence (2) becomes

$$\nabla^2\phi_i = \omega_i. \tag{3}$$

Thus we introduced formally the vector field $\boldsymbol{\phi} = [\phi_i]$ which is homogeneous and isotropic if the vector field $\boldsymbol{\omega}$ is homogeneous and isotropic. We introduce also a two-point correlation tensor

$$G_{ijkl} = \overline{\frac{\partial\phi_i(\boldsymbol{x})}{\partial x_k}\frac{\partial\phi_j(\boldsymbol{x}+\boldsymbol{r})}{\partial x_l}} = -\frac{\partial^2}{\partial r_k\,\partial r_l}\overline{\phi_i(\boldsymbol{x})\,\phi_j(\boldsymbol{x}+\boldsymbol{r})}. \tag{4}$$

The tensor $\overline{\phi_i(\boldsymbol{x})\,\phi_j(\boldsymbol{x}+\boldsymbol{r})}$ has properties analogous to the velocity tensor for an incompressible fluid, since

$$\nabla^2\frac{\partial\phi_j}{\partial x_j} = 0; \quad \overline{\phi_i(\boldsymbol{x})\,\nabla^2\frac{\partial\phi_j(\boldsymbol{x}+\boldsymbol{r})}{\partial x_j}} = 0; \quad \nabla_r^2\left[\frac{\partial}{\partial r_j}\overline{\phi_i(\boldsymbol{x})\,\phi_j(\boldsymbol{x}+\boldsymbol{r})}\right] = 0,$$

and since

$$\overline{\phi_i(\boldsymbol{x})\,\phi_j(\boldsymbol{x}+\boldsymbol{r})} \to 0 \quad \text{for} \quad r\to\infty, \quad \frac{\partial}{\partial r_j}\overline{\phi_i(\boldsymbol{x})\,\phi_j(\boldsymbol{x}+\boldsymbol{r})} = 0,$$

$$\overline{\phi_i(\boldsymbol{x})\,\phi_j(\boldsymbol{x}+\boldsymbol{r})} = -\frac{1}{2r}\frac{\partial F(r)}{\partial r}r_i r_j + \left[F(r) + \tfrac{1}{2}r\frac{\partial F(r)}{\partial r}\right]\delta_{ij}, \tag{5}$$

where $F(r)$ is the longitudinal correlation of the field ϕ_i analogous to the longitudinal correlation $f(r)$ of the velocity field (Hinze 1974, pp. 185–186). From (4) and (5) it follows that

$$\begin{aligned} G_{ijkl} = {} & \left[-\frac{3}{2r^5}\frac{\partial F}{\partial r} + \frac{3}{2r^4}\frac{\partial^2 F}{\partial r^2} - \frac{1}{2r^3}\frac{\partial^3 F}{\partial r^3}\right] r_i r_j r_k r_l + \left[\frac{1}{2r^3}\frac{\partial F}{\partial r} - \frac{1}{2r^2}\frac{\partial^2 F}{\partial r^2}\right] \\ & \times (r_i r_j \delta_{lk} + r_i r_l \delta_{jk} + r_j r_l \delta_{ik} + r_i r_k \delta_{jl} + r_j r_k \delta_{il}) - \frac{1}{2r}\frac{\partial F}{\partial r}(\delta_{ik}\delta_{jl} + \delta_{jk}\delta_{il}) \\ & + \left[-\frac{3}{2r^3}\frac{\partial F}{\partial r} + \frac{3}{2r^2}\frac{\partial^2 F}{\partial r^2} + \frac{1}{2r}\frac{\partial^3 F}{\partial r^3}\right] r_k r_l \delta_{ij} + \left[\frac{3}{2r}\frac{\partial F}{\partial r} + \frac{1}{2}\frac{\partial^2 F}{\partial r^2}\right]\delta_{ij}\delta_{lk}. \end{aligned} \tag{6}$$

Finally we shall need the expression for the two-point second-order velocity correlation tensor (Hinze 1974, p. 186)

$$\overline{u_i(\boldsymbol{x})\,u_j(\boldsymbol{x}+\boldsymbol{r})} = -\frac{1}{2r}\frac{\partial f(r)}{\partial r}r_i r_j + \left[f(r) + \tfrac{1}{2}r\frac{\partial f(r)}{\partial r}\right]\delta_{ij}. \tag{7}$$

We shall make use of (4), (6) and (7) in the following.

2.2. *Intensities* (*r.m.s.*)

Taking derivatives of (3) we obtain

$$\nabla_x^2\overline{\frac{\partial\phi_i(\boldsymbol{x})}{\partial x_k}\nabla_{x+r}^2\frac{\partial\phi_j(\boldsymbol{x}+\boldsymbol{r})}{\partial x_l}} = \overline{\frac{\partial\omega_i(\boldsymbol{x})}{\partial x_k}\frac{\partial\omega_j(\boldsymbol{x}+\boldsymbol{r})}{\partial x_l}}$$

or

$$\nabla_r^4\overline{\frac{\partial\phi_i(\boldsymbol{x})}{\partial x_k}\frac{\partial\phi_j(\boldsymbol{x}+\boldsymbol{r})}{\partial x_l}} = -\frac{\partial^2}{\partial r_k\,\partial r_l}\overline{\omega_i(\boldsymbol{x})\,\omega_j(\boldsymbol{x}+\boldsymbol{r})}. \tag{8}$$

Contraction of the indices $i = j \neq k = l$ in (8) and using the relation $\overline{\omega_i(\boldsymbol{x})\,\omega_i(\boldsymbol{x}+\boldsymbol{r})} = -\nabla_r^2\overline{u_i(\boldsymbol{x})\,u_i(\boldsymbol{x}+\boldsymbol{r})}$ (Batchelor 1953, p. 39) gives

$$\nabla_r^4\overline{\frac{\partial\phi_i(\boldsymbol{x})}{\partial x_k}\frac{\partial\phi_i(\boldsymbol{x}+\boldsymbol{r})}{\partial x_k}} = \nabla_r^4\overline{u_i(\boldsymbol{x})\,u_i(\boldsymbol{x}+\boldsymbol{r})},$$

and finally we obtain the important relation

$$\overline{\frac{\partial \phi_i(x)}{\partial x_k}\frac{\partial \phi_i(x+r)}{\partial x_k}} = \overline{u_i(x)\,u_i(x+r)}. \tag{9}$$

In (8) and (9) we have made use of homogeneity only, therefore the relation (9) is valid for homogeneous non-isotopic turbulence. This makes it possible to measure the energy of turbulence by measuring the nine components $(\partial\phi_i/\partial x_k)^2$ successively (three for every orientation of the magnetic field).

For isotropic turbulence and $r = 0$ it follows from (6) (see also (18*a*, *b*)) that

$$\overline{\left(\frac{\partial \phi_i}{\partial x_k}\right)^2} = \overline{\left(\frac{\partial \phi_i}{\partial x_m}\right)^2}, \quad \overline{\left(\frac{\partial \phi_i}{\partial x_k}\right)^2} = 2\overline{\left(\frac{\partial \phi_j}{\partial x_j}\right)^2},$$

$$i,j,k = 1,2,3; \quad i \neq k, l \neq m, \text{ no summation over } j.$$

This relation could be also obtained from the first part of (4) in precisely the same manner as the analogous relations for the correlations of velocity derivatives replacing u_i by ϕ_i (see equations (18)–(22) in Kármán & Howarth 1938; also Hinze 1974).

From this and (9) it follows that

$$7.5\overline{\left(\frac{\partial \phi_2}{\partial x_3}\right)^2} = 3\overline{u_1^2}, \quad \text{or} \quad \tilde{u}_1 = 1.58\,\widetilde{\frac{\partial \phi_2}{\partial x_3}} \tag{10}$$

and

$$\left.\begin{aligned} \overline{\left(\frac{\partial \phi_2}{\partial x_1}\right)^2} = \overline{\left(\frac{\partial \phi_2}{\partial x_3}\right)^2} &= 2\overline{\left(\frac{\partial \phi_2}{\partial x_2}\right)^2} \\ \text{or} \qquad \widetilde{\frac{\partial \phi_2}{\partial x_1}} = \widetilde{\frac{\partial \phi_2}{\partial x_3}} &= 1.415\,\widetilde{\frac{\partial \phi_2}{\partial x_2}}, \end{aligned}\right\} \tag{11}$$

where $\tilde{}$ indicates the r.m.s. value.

The choice of specific indices in (10) and (11) corresponds to the orientation of the magnetic field along the axis Ox_2 and will be used for the comparison with the experimental results below.

It is clear that (10) represents the precise relation between the velocity intensity and the intensity of one of the components of the electrical field. The relations (11) are important in assessing whether and how far the turbulence deviates from isotropic since these relations are necessary conditions of isotropy (Kolesnikov & Tsinober 1972).

2.3. *Correlations of type* $\overline{u_1(\partial\phi_2/\partial x_3)}$

We start once again from (3)

$$\nabla^2 \phi_k = \omega_k,$$

and multiplying by ω_k one obtains

$$\left.\begin{aligned} \overline{\nabla^2\phi_k(x)\,\epsilon_{ijk}\frac{\partial u_i(x+r)}{\partial x_j}} &= \overline{\omega_k(x)\,\omega_k(x+r)}, \\ \nabla_r^2\,\epsilon_{kji}\overline{\frac{\partial \phi_k(x)}{\partial x_j}u_i(x+r)} &= \nabla_r^2\,\overline{u_k(x)\,u_k(x+r)}, \\ \epsilon_{kji}\overline{\frac{\partial \phi_k(x)}{\partial x_j}u_i(x+r)} &= \overline{u_k(x)\,u_k(x+r)}. \end{aligned}\right\} \tag{12}$$

For the isotropic case and $r = 0$ it follows from (12) that

$$\overline{6\frac{\partial\phi_2}{\partial x_3}u_1} = 3\overline{u_1^2},$$

which together with (10) provides the value of the correlation coefficient between u_1 and the 'corresponding' component of the electrical field $\partial\phi_2/\partial x_3$:

$$\overline{u_1\frac{\partial\phi_2}{\partial x_3}}\Big/\tilde{u}_1\frac{\widetilde{\partial\phi_2}}{\partial x_3} = \tfrac{1}{2}(2.5)^{\frac{1}{2}} = 0.79. \tag{13}$$

In the same manner $$\overline{u_3\frac{\partial\phi_2}{\partial x_1}}\Big/\tilde{u}_3\frac{\widetilde{\partial\phi_2}}{\partial x_1} = -0.79.$$

2.4. *Second-derivative correlations and dissipation-length parameters*

Relations similar to (11) exist for higher derivatives. As we shall see below these relations for the second derivatives are useful in the context of vorticity measurements. It is a matter of simple algebra to obtain one-point correlations between different second derivatives. We will need the following relations:

$$\overline{\frac{\partial^2\phi_2}{\partial x_1^2}\frac{\partial^2\phi_2}{\partial x_3^2}} = \overline{\left(\frac{\partial^2\phi_2}{\partial x_2^2}\right)^2} = \frac{1}{3}\overline{\left(\frac{\partial^2\phi_2}{\partial x_1^2}\right)^2} = \frac{1}{3}\overline{\left(\frac{\partial^2\phi_2}{\partial x_3}\right)^2}; \tag{14a}$$

$$\overline{\frac{\partial^2\phi_2}{\partial x_1^2}\frac{\partial^2\phi_2}{\partial x_2^2}} = \overline{\frac{\partial^2\phi_2}{\partial x_3^2}\frac{\partial^2\phi_2}{\partial x_2^2}} = \frac{2}{9}\overline{\left(\frac{\partial^2\phi_2}{\partial x_3^2}\right)^2}; \tag{14b}$$

$$\overline{\left(\frac{\partial^2\phi_2}{\partial x_1\,\partial x_2}\right)^2} = \frac{2}{9}\overline{\left(\frac{\partial^2\phi_2}{\partial x_3^2}\right)^2}; \tag{14c}$$

$$\overline{\left(\frac{\partial^2\phi_2}{\partial x_1\,\partial x_3}\right)^2} = \frac{1}{3}\overline{\left(\frac{\partial^2\phi_2}{\partial x_3^2}\right)^2}. \tag{14d}$$

These relations are precisely the same as those obtained by Kármán & Howarth (1938) for the second derivatives of velocity components in turbulent isotropic flow.

In checking the performance of the vorticity probe it is useful also to compare the values of the Taylor microscale λ,

$$\lambda^2 = \overline{u_1^2}/\overline{(\partial u_1/\partial x_1)^2} \tag{15a}$$

obtained by different methods. In particular

$$\lambda^2 = 5\overline{u_1^2}/\overline{\omega_2^2} \tag{15b}$$

(Batchelor & Townsend 1947). It is also useful to compare λ with an analogous lengthscale defined as follows:

$$\lambda_3^2 = \overline{\left(\frac{\partial\phi_2}{\partial x_3}\right)^2}\Big/\overline{\left(\frac{\partial^2\phi_2}{\partial x_1\,\partial x_3}\right)^2}. \tag{15c}$$

It follows from (3), (11), (14) and (15*b*) that

$$\lambda^2 = \tfrac{15}{14}\lambda_3^2. \tag{15d}$$

2.5. *Autocorrelations and spectra*

The relation (9) makes it possible to find the longitudinal velocity correlation $f(r)$ by measuring the three components of electric field. We shall obtain this relation by putting $r = r_1$ in (9), (6) and (7) for comparison with the experiments on flow past a

grid, since we made time-correlations measurements and transformed them into space correlations using the Taylor hypothesis.

For $r = r_1$ (9) becomes

$$\overline{u_1(x)\,u_1(x+r_1\,i)} + \overline{2u_2(x)\,u_2(x+r_1\,i)} = \overline{\frac{\partial\phi_1(x)}{\partial x_1}\frac{\partial\phi_1(x+r_1\,i)}{\partial x_1}} + 2\overline{\frac{\partial\phi_1(x)}{\partial x_2}\frac{\partial\phi_1(x+r_1\,i)}{\partial x_2}} + 2\overline{\frac{\partial\phi_2(x)}{\partial x_k}\frac{\partial\phi_2(x+r_1\,i)}{\partial x_k}}, \quad (16)$$

and from (6) and (7) it follows that

$$\overline{u_1(x)\,u_1(x+r_1\,i)} = f(r_1), \quad (17a)$$

$$\overline{u_2(x)\,u_2(x+r_1\,i)} = f(r_1) + \tfrac{1}{2}r_1 f'(r_1); \quad (17b)$$

$$\overline{\frac{\partial\phi_1(x)}{\partial x_1}\frac{\partial\phi_1(x+r_1\,i)}{\partial x_1}} = F''(r_1), \quad (18a)$$

$$\overline{\frac{\partial\phi_1(x)}{\partial x_2}\frac{\partial\phi_1(x+r_1\,i)}{\partial x_2}} = \frac{2}{r_1}F'(r_1), \quad (18b)$$

$$\overline{\frac{\partial\phi_2(x)}{\partial x_1}\frac{\partial\phi_2(x+r_1\,i)}{\partial x_1}} = 2F''(r_1) + \tfrac{1}{2}r_1 F'''(r_1), \quad (18c)$$

$$\overline{\frac{\partial\phi_2(x)}{\partial x_2}\frac{\partial\phi_2(x+r_1\,i)}{\partial x_2}} = \frac{1}{2r_1}F'(r_1) + \tfrac{1}{2}F''(r_1), \quad (18d)$$

$$\overline{\frac{\partial\phi_2(x)}{\partial x_3}\frac{\partial\phi_2(x+r_1\,i)}{\partial x_3}} = \frac{3}{2r_1}F'(r_1) + \tfrac{1}{2}F''(R_1). \quad (18e)$$

The relation between $F(r_1)$ and $f(r_1)$ follows from (16), (17*a*, *b*) and (18*a*–*e*) (and it also follows directly from (5), (7) and (9)):

$$3f + r_1 f' = \frac{8}{r_1}F' + 7F'' + r_1 F''', \quad (19)$$

In the experiments we measure the three components of the electric field which appear in (18*c*–*e*). From these relations the derivatives of $F(r_1)$ are expressed in terms of correlations of the electrical field and inserted in (19). Finally, solving (19) with (10) as a condition at $r = 0$, we obtain an expression for calculating $f(r_1)$ from the experimental data for the electrical field:

$$f(r) = r^{-3}\int_0^r \rho^2\left[2\overline{\frac{\partial\phi_2(x)}{\partial x_1}\frac{\partial\phi_2(x+\rho i)}{\partial x_1}} + \overline{\frac{\partial\phi_2(x)}{\partial x_2}\frac{\partial\phi_2(x+\rho i)}{\partial x_2}} + 5\left(\overline{\frac{\partial\phi_2(x)}{\partial x_3}\frac{\partial\phi_2(x+\rho i)}{\partial x_3}}\right)\right]\mathrm{d}\rho. \quad (20)$$

3. Experiments and comparison with theory

3.1. *Facility, instrumentation, data acquisition and processing*

The experiments were performed with salted water (salinity $\approx 1\,\%$) in a constant-head facility with the test section 5 cm × 5 cm in cross-section and 1.2 m in length. The use of salted water (low electrical conductivity) ensured that the dynamic interaction of the flow and the magnetic field is entirely negligible (which is not the case

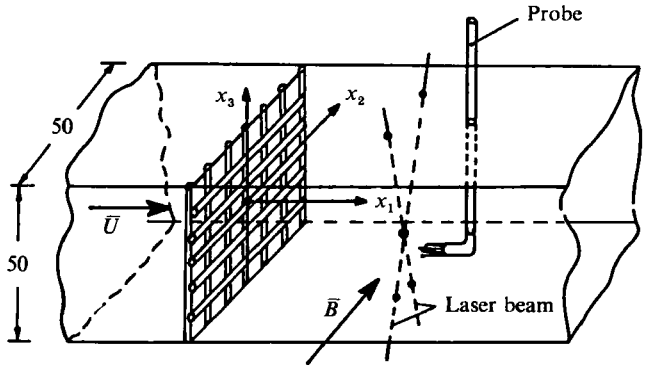

FIGURE 1. Schematic of the experimental arrangement of the test section.

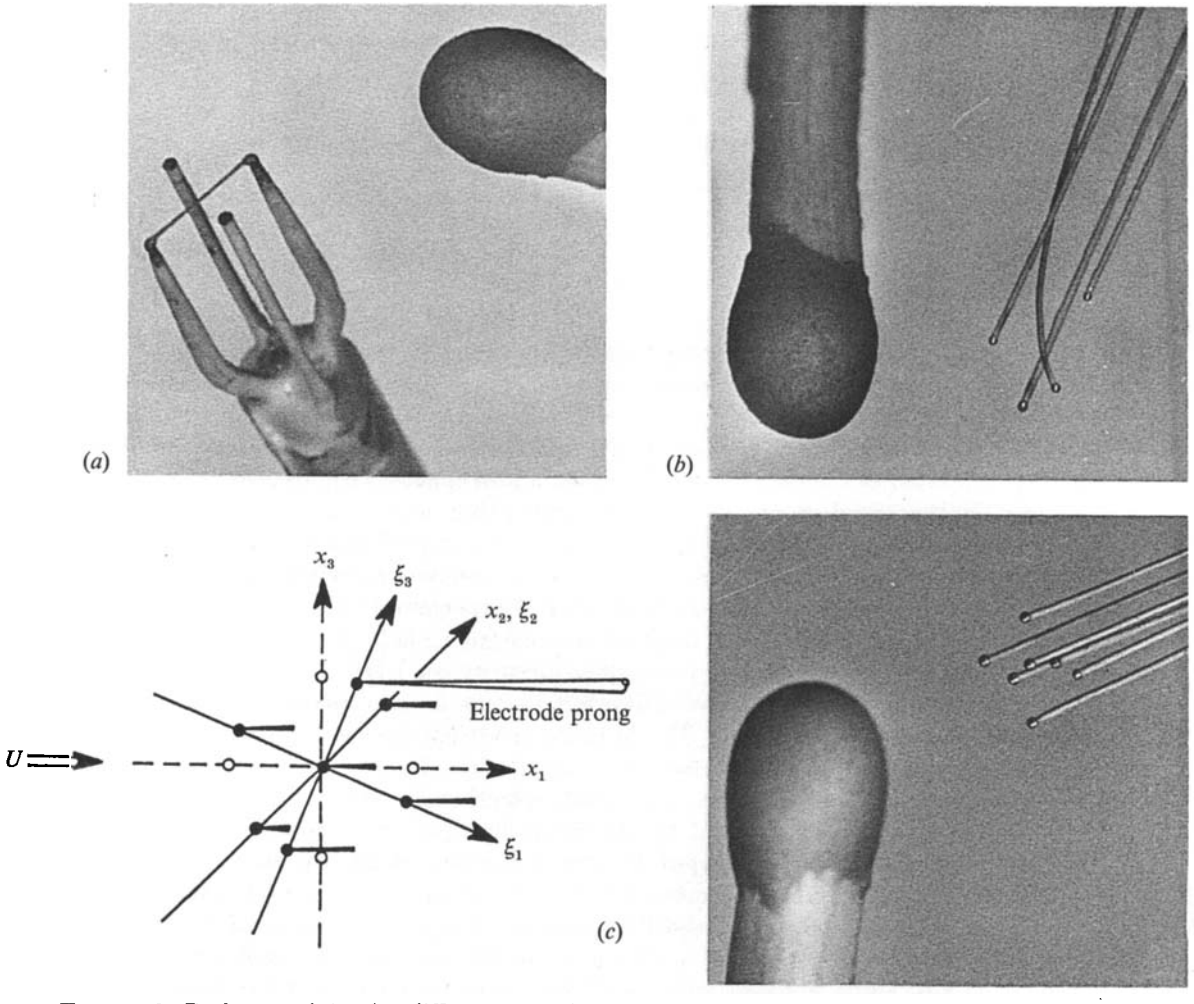

FIGURE 2. Probes used in the different experiments: (*a*) a two-electrode probe with a hot-film-wire-type probe; (*b*) a four-electrode probe; (*c*) a schematic of the tip of a seven-electrode vorticity probe. The seven tips of the electrodes in the plane x, Ox_3 are turned 22.5° relative to the Ox axis in order to minimize the disturbances between them. On the right one of the probes is shown together with head of a match.

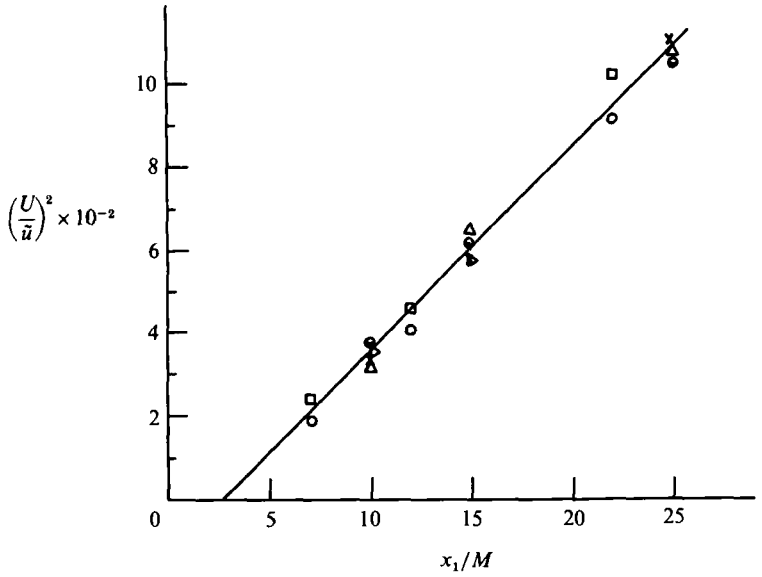

FIGURE 3. Decay of intensity of turbulence measured by: ○, $\tilde{u}_1$, hot-film wire-type, $U = 67$ cm/s; △, $\tilde{u}_1$, conical hot-film, $U = 67$ cm/s; □, $(2.5)^{\frac{1}{2}}\frac{\widetilde{\partial\phi}}{\partial x_3}$, two-electrode probe, $U = 67$ cm/s. ◒, ×, ▷, $(2.5)^{\frac{1}{2}}\frac{\widetilde{\partial\phi}}{\partial x_3}$, seven-electrode vorticity probe; $U = 50$ cm/s, 67 cm/s and 115 cm/s respectively.

with liquid metals), since for salted-water flow even in very strong magnetic fields the electromagnetic force is several orders of magnitude smaller than the viscous and inertia forces.

The experimental arrangement of the test section is shown in figure 1. We used a grid composed of circular rods of diameter 5 mm spaced with 10 mm between their centres. Some experiments were made with other grids and without grids. The turbulence level in the oncoming flow in front of the grid was reduced to below 1% by a system of small-scale screens. Most of the experiments were performed with the mean velocity $u = 67$ cm/s. A small number of experiments were made for velocities between 30 and 115 cm/s. The imposed d.c. magnetic field $B = 0.5$ tesla.

The u_1 component of velocity was measured by an LDV meter and/or hot-film anemometer. The hot film was calibrated *in situ* in the turbulent flow using an iterative calibration procedure. The induced electrical field was measured by multi-electrode probes consisting of two, four and seven electrodes. Specially processed silver–silver chloride electrodes were used, which made it possible to reduce their electrochemical offset potential to the noise level of the electronics used in the experiments (0.3 μv to the input in the frequency range up to 200 Hz). Since electrodes of this kind are photosensitive (to intense light) it was very difficult to use LDV together with the potential-difference probe for measurements of the one-point correlation between $\partial\phi/\partial x_3$ and u_1. To measure this correlation a probe consisting of two electrodes and a hot film (wire type) was constructed (figure 2*a*). Simultaneous measurements of the three components $\partial\phi/\partial x_i$ $(i = 1, 2, 3)$ of the electrical field were made by a four-electrode probe (figure 2*b*). Some of these measurements were made by a probe consisting of four electrodes and a conical hot-film probe. The seven-electrode probe was used to produce a central-difference approximation of the

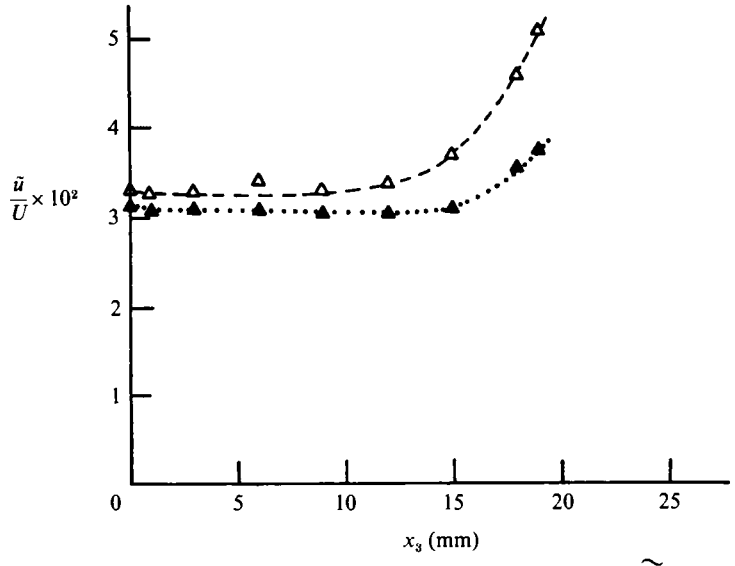

FIGURE 4. An example of distribution of velocity intensity and $\frac{\partial\tilde{\phi}}{\partial x_3}$ along the Ox_3 direction. $x_1 = 25$ cm. △, $\tilde{u}$ measured with wire hot film; ▲, $\tilde{u} = (2.5)^{\frac{1}{2}}\frac{\partial\tilde{\phi}}{\partial x_3}$ measured with potential-difference probe.

Laplacian $\nabla^2\phi$ which allowed the vorticity component parallel to the imposed magnetic field to be measured. To minimize the mechanical contamination of the signal the approximating grid was turned 22.5° in the (x, z)-plane (figure 2*c*). This is possible owing to the invariance of a Laplace operator to rotation. The distance between the tips of the electrodes was 1 mm (the electrode diameter being 0.1 mm) for the vorticity probe (seven electrodes, figure 2*c*). For all the other probes the distance between the tips of the electrodes was 2 mm.

The data (up to eight channels in total) were acquired by a PDP 11/23+ minicomputer and recorded on magnetic tape. The sampling rate was from 250 Hz to 1 kHz per channel. The minimal buffer length was 512 points per channel to facilitate data processing by a fast Fourier transform to obtain the spectra and correlation functions. The record of almost every experimental point consisted of 50 buffers, so that all the data (intensities, correlations and spectra) were obtained as the result of ensemble averaging over these 50 buffers.

3.2. *Intensities, correlations and spectra*

The data showing the decay law of intensities of streamwise velocity fluctuations and the components of the induced electrical field in the centre of the channel cross-section are shown in figure 3 (U is the mean velocity measured independently by a flow meter). The behaviour of the quantity $(U/\tilde{u})^2$ versus x/M (M is the mesh size of the grid) is in agreement with previous results (Batchelor & Townsend 1947; Tan-Atichat, Nagib & Loehrke 1982).

It is easy to see from figure 3 that (10) is well satisfied in the centre of the cross-section. This relation is confirmed in the central part of the cross-section as can be seen from figure 4, where it is demonstrated along the x_3 axis at $x_1 = 25$ cm. It is also seen from this figure that the flow becomes anisotropic when the distance from

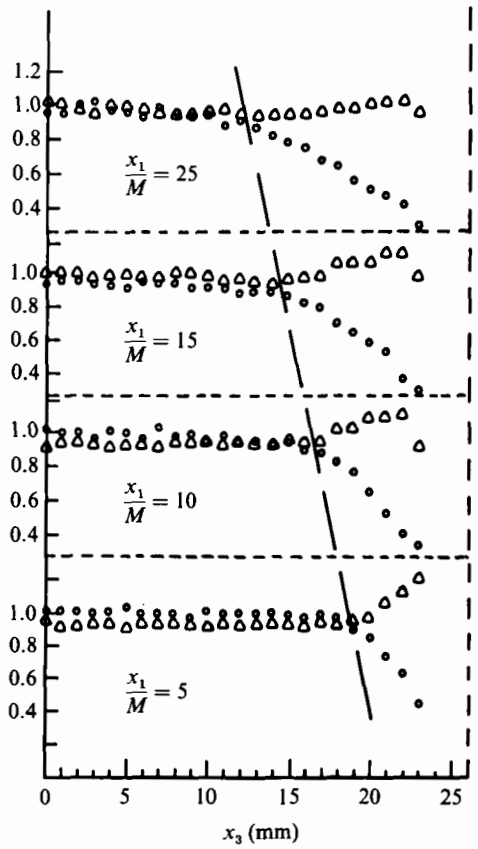

FIGURE 5. Checking the isotropy relations along the flow cross-section at different distances from the grid. △, $\widetilde{\frac{\partial\phi}{\partial x_3}} \Big/ \sqrt{2}\widetilde{\frac{\partial\phi}{\partial x_2}}$; ○, $\widetilde{\frac{\partial\phi}{\partial x_1}} \Big/ \widetilde{\frac{\partial\phi}{\partial x_3}}$.

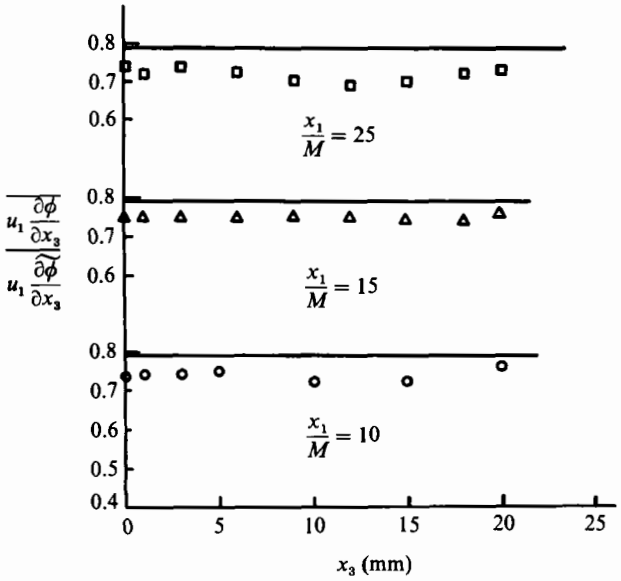

FIGURE 6. Verification of the relation (13).

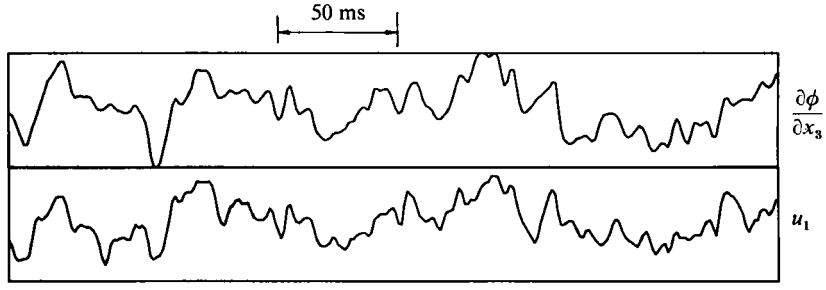

FIGURE 7. An example of oscillograms of the u_1 signal measured by a wire hot-film probe and of the $\partial\phi/\partial x_3$ signal measured by the potential-difference probe.

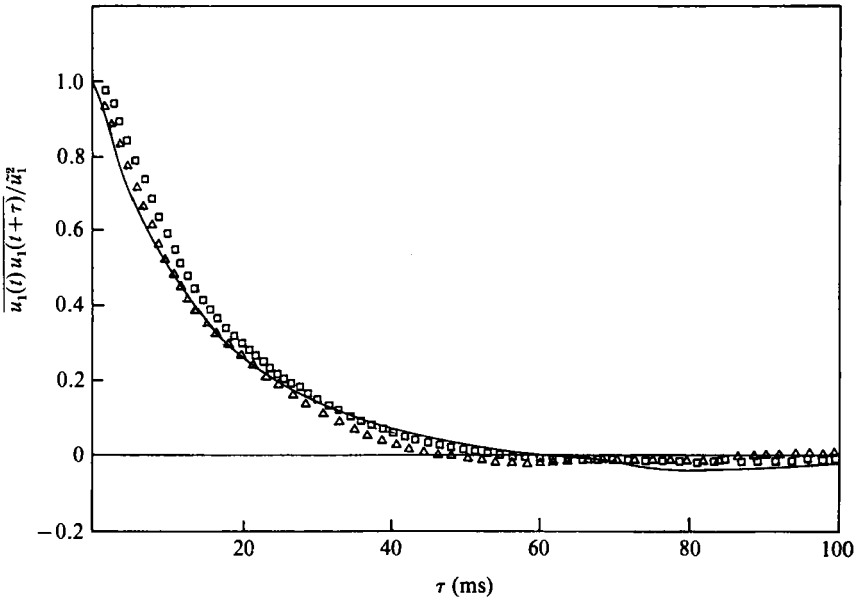

FIGURE 8. Velocity autocorrelation function obtained by diffeent methods as a check of relation (20). $x_1 = 10$ cm, $x_2 = 0$. ——, direct laser-Doppler measurement; □, calculated from measurements of the three components of the electrical field; △, $2.5\overline{(\partial\phi(t)/\partial x_3)(\partial\phi(t+\tau)/\partial x_3)}/\tilde{u}_1^2$.

the wall decreases. Figure 5 illustrates the increasing influence of the walls and the decrease of the region of flow isotropy with the distance from the grid on the basis of (11) which, as mentioned above, is one of the necessary conditions of flow isotropy.

Measurements of the correlation coefficient defined in (13) in the centre of the flow cross-section produced the value 0.74 ± 0.1, which is very good compared with the theoretical value 0.79. It is interesting that this coefficient remains almost constant along the x_3 direction up to $x_3 \approx 20$ mm from the centreline (figure 6). An example of oscillograms of the signals of both u_1 and $\partial\phi/\partial x_3$ shown in figure 7 demonstrates clearly their similarity in conformity with the high value of their correlation coefficient.

The autocorrelation $\overline{u_1(t)\,u_1(t+\tau)}/\tilde{u}_1^2$ obtained by three different methods is shown in figure 8. It is seen quite clearly that both calculations from (20) and $2.5\,\overline{(\partial\phi(t)/\partial x_3)\,(\partial\phi(t+\tau)/\partial x_3)}/\tilde{u}_1^2$ are in good agreement with the direct laser-Doppler measurements.

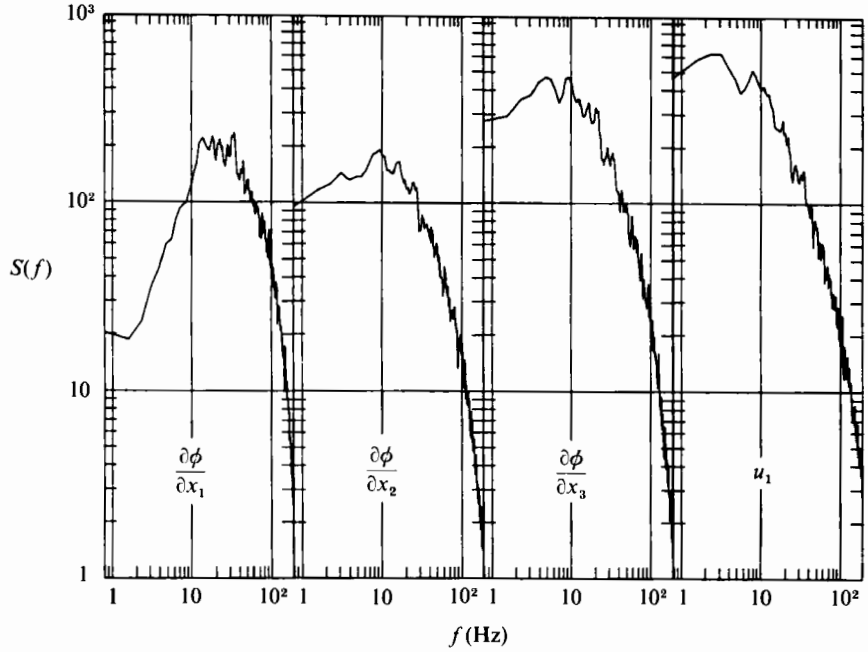

FIGURE 9. One-dimensional spectra of velocity u_1 and electrical-field components $\partial\phi/\partial x_3\,(i = 1, 2, 3)$.

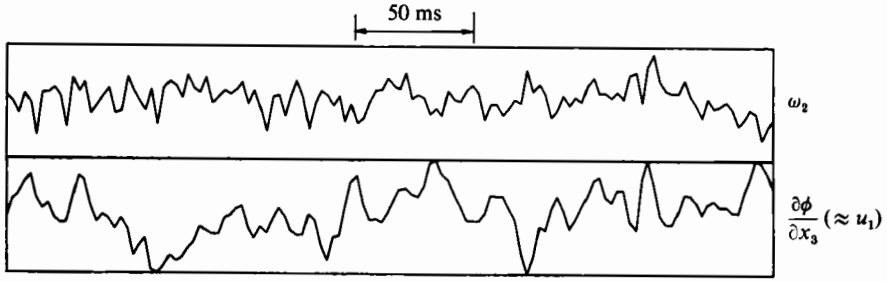

FIGURE 10. Comparing of oscillograms of simultaneous signals ω_2 and $\partial\phi/\partial x_3\,(\approx u_1)$ illustrating larger content of high frequencies in the ω_2 signal.

It is seen from (20) that the largest contribution to the integral is from $\overline{(\partial\phi(t)/\partial x_3)\,(\partial\phi(t+\tau)/\partial x_3)}$ and this is believed to be the reason for the good agreement between the two quantities $\overline{u_1(t)\,u_1(t+\tau)}/\tilde{u}^2$ and $2.5\,\overline{(\partial\phi(t)/\partial x_3)\,(\partial\phi(t+\tau)/\partial x_3)}/\tilde{u}_1^2$.

For the same reason the one-dimensional spectra of u_1 and $\partial\phi/\partial x_3$ are very similar, as is seen from figure 9.

3.3. *Preliminary measurements of vorticity and related quantities*

Oscillograms of simultaneous signals of ω_2, the vorticity component parallel to the magnetic field, and $\partial\phi/\partial x_3$† are shown in figure 10. It is clearly seen that the ω_2 signal contains much more high frequencies than $\partial\phi/\partial x_3$, which could be considered as

† Note that the derivatives $\partial\phi/\partial x_1 = (\partial\phi/\partial\xi_1)\cos 22.5° - (\partial\phi/\partial\xi_3)\sin 22.5°$; $\partial\phi/\partial x_3 = (\partial\phi/\partial\xi_1) \times \sin 22.5° + (\partial\phi/\partial\xi_3)\cos 22.5°$.

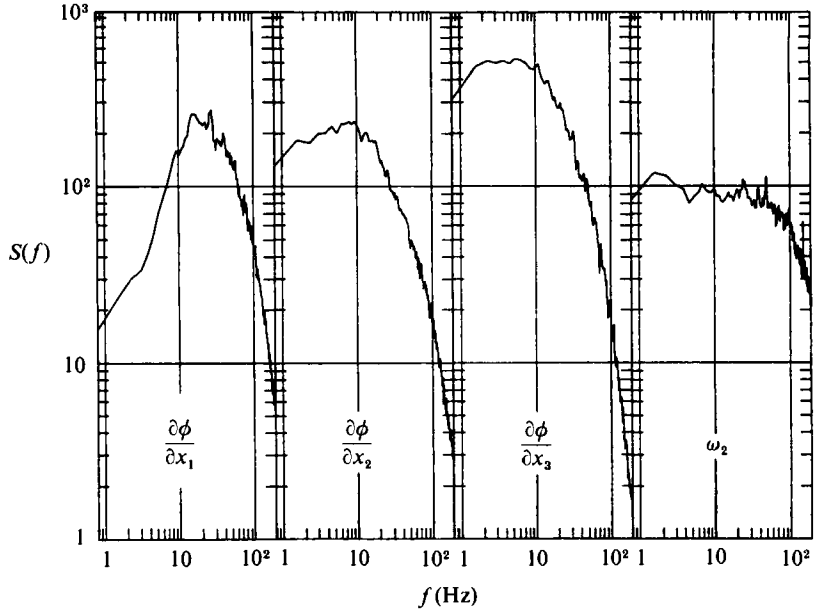

FIGURE 11. One dimensional spectra of ω_2 and electrical-field components $\partial\phi/\partial x_i\,(i = 1, 2, 3)$.

$\frac{x}{M}$	$\frac{\overline{\left(\frac{\partial^2\phi}{\partial\xi_1^2}\right)^2}}{\left(\frac{\partial^2\phi}{\partial\xi_3^2}\right)^2}$	$\frac{\overline{\left(\frac{\partial^2\phi}{\partial\xi_2^2}\right)^2}}{\left(\frac{\partial^2\phi}{\partial\xi_3^2}\right)^2}$	$\frac{\overline{\frac{\partial^2\phi}{\partial\xi_1^2}\frac{\partial^2\phi}{\partial\xi_3^2}}}{\left(\frac{\partial^2\phi}{\partial\xi_3^2}\right)^2}$	$\frac{\overline{\frac{\partial^2\phi}{\partial\xi_1^2}\frac{\partial^2\phi}{\partial\xi_2^2}}}{\left(\frac{\partial^2\phi}{\partial\xi_3^2}\right)^2}$	$\frac{\overline{\frac{\partial^2\phi}{\partial\xi_2^2}\frac{\partial^2\phi}{\partial\xi_3^2}}}{\left(\frac{\partial^2\phi}{\partial\xi_3^2}\right)^2}$	$\frac{\overline{\left(\frac{\partial^2\phi}{\partial x_1\,\partial x_2}\right)^2}}{\left(\frac{\partial^2\phi}{\partial x_1^2}\right)^2}$	$\frac{\overline{\left(\frac{\partial^2\phi}{\partial x_1\,\partial x_3}\right)^2}}{\left(\frac{\partial^2\phi}{\partial x_1^2}\right)^2}$
10	0.80	0.360	0.332	0.188	0.223	0.376	0.44
15	0.82	0.351	0.327	0.192	0.214	0.361	0.43
25	0.92	0.324	0.362	0.224	0.222	0.322	0.40
Theoretical value	1	$\frac{1}{3}$	$\frac{1}{3}$	$\frac{2}{9}$	$\frac{2}{9}$	$\frac{2}{9}$	$\frac{1}{3}$

TABLE 1. Verifying the isotropy relations (14) for the second derivatives of the potential of the electrical field

representing the u_1 velocity signal (see figure 7). The same is seen from an example of one-dimensional spectra (figure 11).

As a test of the vorticity-probe performance the isotropy relations (14*a–d*) were checked from the measurements of the second derivations of ϕ in the frame $O\xi_1\,\xi_2\,\xi_3$. The results are shown in table 1 and are quite reasonable bearing in mind that we made a rather crude approximation of the second derivatives. Also in this table are results for the derivatives $(\partial^2\phi/\partial x_1\,\partial x_i) = (\partial/\partial x_1)\,(\partial\phi/\partial x_i), (i = 1, 2, 3)$ in which the $\partial/\partial x_i$ were obtained as mentioned above, and $\partial/\partial x_1$ using the Taylor hypothesis.

The results of calculations of the dissipation lengthscale from the relations (15*a–d*) are presented at figure 12 together with a line of theoretical slope $\mathrm{d}\lambda^2/\mathrm{d}x = 10\nu/U$ (Batchelor & Townsend 1947). Though the scatter is considerably large the tendency seems to be the right one.

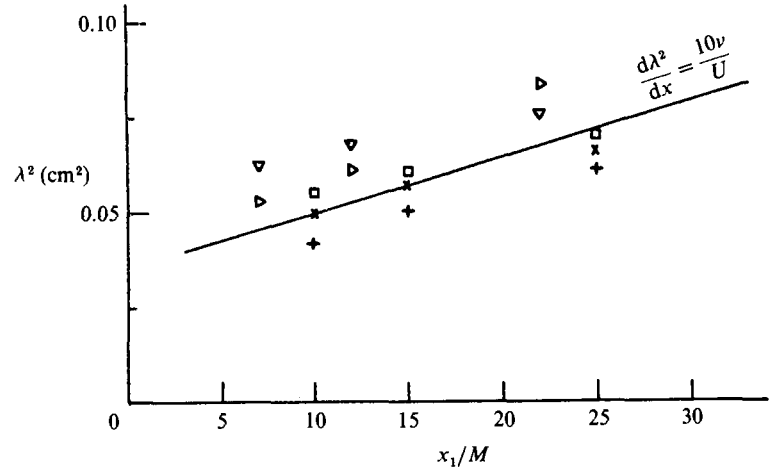

FIGURE 12. Variation of dissipation lengthscale during decay: +, equation (15*a*), conical hot film; ▷, (15*b*), wire hot film; ▽, (15*c*), two-electrode probe; □, (15*d*), four-electrode probe; ×, (15*b*), seven-electrode vorticity probe.

4. Discussion and concluding remarks

It has been shown that for homogeneous and isotropic turbulence there exist precise relations between statistical characteristics of turbulent velocity and an electrical field (relations (10), (13)). These include the relation for the two-point velocity correlations as defined by the longitudinal (and correspondingly the transverse) velocity correlation function $f(r)$ which is found by simple integration from measurements of the three components of the electrical field (relation (20)).

Another important result is that measurements of the three components of the electrical field $\partial\phi/\partial x_i$ and/or their derivatives $\partial^2\phi/\partial x_i\,\partial x_j$ makes it possible to assess the deviation of turbulence from isotropy relations (11), (14).

We made an attempt to verify these relations in a flow past a grid of high solidity (0.75). This allowed a high turbulence level to be obtained and large-scale and slow turbulence decay (Tan-Atichat *et al.* 1982). Most of the experiments exhibited good agreement with theoretical results for isotropic turbulence despite a rather crude technique of simulation of isotropic homogeneous turbulence.

The most pressing problem is that the resolution scale of the potential-difference probes ($\approx$ 1 mm) was not small enough in comparison with the grid mesh (5 mm). This is especially important when the measurement of vorticity and related quantities (like $\partial^2\phi/\partial x_i\,\partial x_j$) is attempted. For this reason the vorticity measurements presented here should be considered as preliminary only. However, these measurements seem to show the right trends qualitatively as, for example, could be seen from the spectra shapes in the high-frequency region (figure 11) and the dissipation-lengthscale behaviour. To obtain more reliable results it is necessary to increase the scale separation. (A large-scale facility is currently under construction.) It is noteworthy that the main advantage of the presented method of vorticity measurements is that it does not require calibration and it is applicable to any flow (not only isotropic).

In conclusion we should like to mention that though the potential-difference method is generally unable to provide precise information on the velocity field (except for homogeneous and isotropic turbulence) it has some advantages compared with

other methods for turbulence measurements. Some of them are as follows: (i) the possibility of distinguishing between velocity components due to the vector nature of the basic relation and sensitivity to the direction of the flow; (ii) it is linear and does not require any calibration procedure (in fact no calibration procedure can be applied to this method); (iii) it is insensitive to the physical properties of the fluid medium; (iv) it yields an instantaneous measure of quantities fluctuating in time, i.e. its response time is extremely small; (v) it operates in flows of a complex nature (recirculating flows, flows without mean velocity, flows with varying temperature), and it allows the determination of the separation and reattachment points and the moment and position of the turbulence onset or relaminization; and, finally, (vi) the method could be used in non-isotropic turbulence for determining the spectral interval where the turbulence becomes locally isotropic by using high-pass filters and checking if the relations (11) and (14) are valid.

The support of the Israeli National Council of Research and Development is greatly appreciated.

REFERENCES

BAKER, R. C. 1971 On the electromagnetic vortex probe. *J. Phys.* E: *Sci. Instrum.* **4**, 99–101.

BAKER, R. C. 1983 A review of recent developments in electromagnetic flow measurement. *Prog. Astronaut. Aeronaut.* **84**, 225–259.

BATCHELOR, G. K. 1953 *The Theory of Homogeneous Turbulence.* Cambridge University Press.

BATCHELOR, G. K. & TOWNSEND, A. A. 1947 Decay of vorticity in isotopic turbulence. *Proc. R. Soc. Lond.* A **190**, 534–550.

GROSSMAN, L. M., LI, H. & EINSTEIN, H. 1958 Turbulence in civil engineering. Investigation of liquid shear flow by electromagnetic induction. *J. Hydraul. Div. ASCE* **83**, 1–15.

HINZE, T. O. 1974 *Turbulence.* McGraw Hill.

KÁRMÁN, T. VON & HOWARTH, L. 1938 On the statistical theory of isotropic turbulence. *Proc. R. Soc. Lond.* A **164**, 192–215.

KIT, L. G. 1970 Turbulent velocity fluctuation measurements using a conduction anemometer with three-electrode probe. *Magnetohydrodyn.* **6**, 480–487.

KOLESNIKOV, YU. B. & TSINOBER, A. B. 1972 Two dimensional turbulent flow behind a circular cylinder. *Magnetohydrodyn.* **8**, 300–307.

LANCASTER, R. W. 1985 Current profiling in near real time. *Sea-Technol.* **26**, No. 2, 24–28.

RICOU, R. & VIVES, C. 1982 Local velocity and mass transfer measurement in molten metals using an incorporated magnet probe. *Intl J. Heat Mass Transfer* **25**, 1579–1588.

SHERCLIFF, J. A. 1962 *The Theory of Electromagnetic Flow Measurement.* Cambridge University Press.

TAN-ATICHAT, T., NAGIB, H. M. & LOEHRKE, R. L. 1982 Interaction of free-stream turbulence with screens and grids: a balance between turbulence scales. *J. Fluid Mech.* **114**, 501–528.

WEISSENFLUH, T. VON 1985 Probes for local velocity and temperature measurements in liquid metal flow. *Intl J. Heat Mass Transfer* **28**, 1563–1574.